Adhesion-induced reorganization of charged fluid membranes

J. Nardi,[1] R. Bruinsma,[2] and E. Sackmann[1,*]
[1]*Biophysics Group, Physik Department, Technische Universität München, James-Franck-Strasse, D-85748 Garching, Germany*
[2]*Physics Department, University of California at Los Angeles, Los Angeles, California 90024*
(Received 9 February 1998)

Adhesion between simple single-component membranes is both theoretically and experimentally well understood. We report on a combined theoretical and experimental study of the adhesion between well-characterized multicomponent membranes. In particular, we examined the statics and dynamics of the adhesion between a cationic vesicle and an anionic supported membrane on a substrate with a *p*H adjustable surface charge. Through interferometric methods, we measured the adhesion-induced membrane tension. We find a dramatic breakdown of the classical Young-Dupré law at higher surface charge densities. The failure of the Young-Dupré law is associated with the formation of blisters. These results are in agreement with a thermodynamic analysis of anion-cation adhesion which predicts that adhesion-induced phase separation leads to reorganization of the adhesion disk and to a failure of the Young-Dupré law. Our study demonstrates that adhesion of multicomponent membranes is fundamentally different from that of single-component membranes. [S1063-651X(98)15610-6]

PACS number(s): 87.22.Bt, 64.75.+g

I. INTRODUCTION: ADHESION OF MULTICOMPONENT MEMBRANES

Biological membranes are two-dimensional multicomponent materials which play a central role as partitioning surfaces in cells [1]. The main constituent material of biomembranes is amphiphilic phospholipid. In a typical biomembrane many different types of lipids are encountered with a variety of attached alkane chains and a variety of headgroup areas [2], while the headgroups may or may not be charged. Moreover, biomembranes also contain substantial amounts of cholesterol and functional proteins. Finally, membrane proteins may penetrate the membrane completely (integral membrane proteins), or they may be associated with the membrane through a lipid anchor or by physisorption.

Studies of physical properties of membranes have mostly centered on single-component monolayers or bilayers, since such ''model membranes'' are easiest to characterize. This restriction may, however, neglect important physical phenomena which are only present in multicomponent membranes. Numerous experimental studies of the phase behavior of both artificial and natural membranes [3] indicate that the lipid moiety of the biomembranes is, in general, rather close to a phase separation threshold or to a demixing point. The importance of this observation lies in the fact that proximity to a phase separation boundary may allow membrane processes to be regulated in a very flexible way, namely, by the formation of functional entities through local forms of phase separation. Examples are the following:

(i) The lipid-mediated aggregation of integral membrane proteins by the selective attraction of the proteins to certain lipids [3,4]. The driving force for the phase separation here is the mismatch in length between the hydrophobic cores of the protein and that of the lipids constituting the mixed bilayer.

(ii) Phase separation of negatively charged lipids due to adsorption of positively charged proteins or of polyvalent cations [3,4,5]. The driving force for the phase separation here is electrostatic attraction. A prominent case is the Ca^{2+}-induced fusion of synaptic vesicles with the presynaptic membrane [1]. Protein-induced phase separation of artificial membranes is in fact used in a practical manner as a chromatography method [6].

In this paper we present the results of a combined theoretical and experimental study of the role of phase separation for a process which is of considerable biological importance, namely, membrane adhesion. Adhesion between artificial single-component membranes is controlled by the competition between various interaction potentials: van der Waals attraction [7], double-layer electrostatic repulsion [7], and hydration forces [7]. In addition, entropic—or Helfrich—repulsion [8] can prevent adhesion due to thermal fluctuations. Cellular adhesion, on the other hand, is well known to proceed differently, namely, via formation of small, dense adhesion domains (sometimes called adhesion plaques) of receptor-ligand pairs. Specific lock-and-key recognition of receptor-ligand pairs plays a fundamental role for tissue development and immunology [1]. Although suggestive, it is currently not known whether adhesion plaques of biomembranes form through an adhesion-driven form of phase separation.

Motivated by these questions, we have studied a simple model system for the adhesion of a multicomponent membrane in the form of vesicles containing low concentrations of anionic lipids. The vesicles were placed in contact with a flat support covered by a membrane carrying a low concentration of complementary cationic lipids. The vesicles were large enough to allow us to follow the kinetics of the adhesion process by interferometry. In addition, since both the anionic vesicle and the cationic flat membrane were simple binary mixtures of neutral and charged lipids, analytical treatment of both the thermodynamic and kinetic aspects of the adhesion process is possible, so that the experimental

*Author to whom correspondence should be addressed. Electronic address: sackmann@physik.tu-muenchen.de

results could be compared with theory. A brief report of our results was published earlier [9].

The positively and negatively charged lipids perform here a dual role: if the lipids are fully mixed and in a mobile state, they provide an attractive electrostatic interaction potential per unit area (at least for spacings large compared to the Debye screening length). Adhesion in this regime is similar to that of single-component membranes. On the other hand, if the two membranes are in close contact the lipids could demix, forming dense plaques of anions and cations, which could either resemble an array of salt bridges or a two-dimensional Wigner crystal of positive and negative charges. Adhesion in this regime could be considered as a simple model for receptor-ligand adhesion of biomembranes. Both forms of adhesion thus could be realized by our model system.

These two adhesion scenarios can be monitored at a fundamental thermodynamic level through Young's law,

$$S=\gamma(1-\cos\ \vartheta_c), \tag{1}$$

with S the so-called spreading pressure [10], γ the adhesion-induced membrane tension, and ϑ_c the nominal contact angle between the vesicle and the substrate. It is customary to identify S with the specific adhesion energy W of the two membranes. By that we mean that W is the work per unit area required to separate the two surfaces for fixed concentrations of the materials of which the two surfaces are composed. The resulting expression is known as the Young-Dupré law. We will show that if the adhesion process does not lead to phase separation then S is indeed equal to the specific adhesion energy W. If, on the other hand, the anionic lipids segregate out toward the adhesion disk, then the spreading pressure is, as we will show, in general quite different from W. By monitoring the ratio S/W, we can in principle examine the role of phase separation during adhesion. An important aim of this paper is to demonstrate that measurement of the S/W ratio can be a practical tool to distinguish the different forms of adhesion.

Our paper is organized as follows. In Sec. II we present a theoretical discussion of the thermodynamic and kinetic aspects of adhesion between oppositely charged binary membranes using a simple continuum theory. Continuum theory predicts that *tight adhesion between membranes in the mixed state is in general impossible*: the equilibrium intermembrane spacing $l^\star$ is on the order of the Debye screening length. An exception is formed by so-called charge-regulated ''anionic-cationic membrane pairs,'' which have an equal but opposite surface charge. In this case $l^\star$ is a molecular length. Above a—quite low—threshold for the surface charge density, the uniform mixed state is predicted to be unstable against phase separation. The phase separation is predicted to partition the vesicle into a charge-regulated adhesion disk and a charge-depleted exterior section.

Phase separation is not the only possible scenario to lead to charge regulation. Changes induced in the ion-dissociation rates of the lipid molecules by the electrostatic potential are well known to be able to produce charge regulation without requiring any phase separation [11,12]. Charge regulation by phase separation appears to be the route favorable for the experimental conditions discussed below, but in general both scenarios are possible.

The kinetics of this decomposition process can be studied theoretically using linear response theory. Linear response theory predicts that decomposition should be accompanied by the transport of coions and counterions from regions of strong adhesion to regions of weak adhesion by the dialytic action of the membrane. As a consequence, a weak-adhesion area surrounded by a belt of strong, charge-regulated adhesion should trap excess salt. The resulting osmotic pressure should lead to pressurization of the weak-adhesion areas, which will be shaped like spherical caps (''blisters'').

In Sec. III we present our experimental procedure to test the theory and to measure the S/W ratio. In the supported membrane we use pH-sensitive cationic lipids which allow us to increase the surface charge density while monitoring the adhesion area by reflection interference contrast microscopy (RICM). By analyzing the membrane at the blisters and at the edge of the adhesion disk, we measured the tension and contact angle. We then determined the spreading pressure S using Eq. (1), and compared it with the theoretical value of the specific adhesion energy W for electrostatically coupled membranes. We found that upregulation of the surface charge density of the supported membrane indeed led to the formation of pressurized blisters (see Fig. 9), as predicted by the kinetic theory. The ratio S/W was of order 10^{-3} in this regime. At low surface charge densities, no blistering was observed. In this regime, the Young-Dupré law [i.e., Eq. (1), with $S\cong W$] was found to be approximately correct. The critical surface charge density σ^* separating the two regimes is consistent with the theoretically predicted value quoted in Sec. II.

The results of our study thus suggest that at least for our multi-component model membrane, there are indeed two fundamentally different forms of adhesion possible. One regime, in which adhesion follows the Young-Dupré law, where the phenomenology of adhesion is essentially correct and one in which the Young-Dupré law is seriously violated (i.e., $S\ll W$), and which is characterized by adhesion-induced demixing.

II. THEORY

A. Adhesion thermodynamics

As discussed in Sec. I we need to know the specific adhesion energy W for electrostatic attraction between charged surfaces. In this section we will examine the equilibrium thermodynamics of two oppositely charged membranes with the purpose of computing W. Assume the geometry of Fig. 1: two flat, parallel charged fluid membranes that have uniform surface charge densities $\sigma_1<0$ and $\sigma_2>0$. The spacing between the two membranes is denoted by h. We will assume that the aqueous medium inside the gap contains added salt with a concentration c. The dielectric constant of the slabs bordering the gap is assumed to be small compared to that of water. We will assume that the positive surface charges are mobile while the negative charges are fixed.

The simplest method to compute the specific adhesion energy W is to use the Debye-Hückel (DH) theory. The electrostatic force per unit area $P(h)$ between the two membranes (''disjoining pressure'') was computed by Parsegian and Gingell within DH theory, with the result [13]

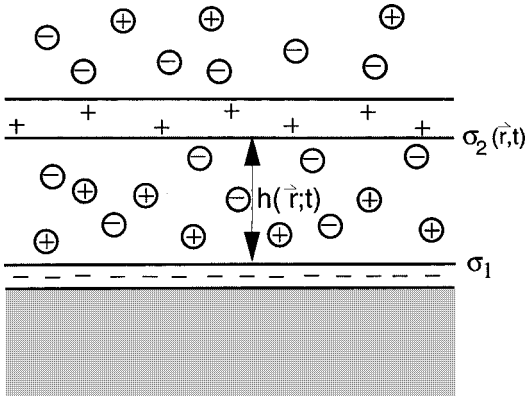

FIG. 1. Two flat, parallel, charged membranes with surface charge densities σ_1 and σ_2 of opposite sign ($\sigma_1<0$, $\sigma_2>0$ and $|\sigma_1|>\sigma_2$). The lipids in the lower membrane are fixed, whereas those in the upper membrane are mobile. The distance between the two membranes is h. The aqueous medium contains salt [symbolized by $(-)$ and $(+)$] of concentration c.

$$P(h)=\frac{8\pi}{\varepsilon}\frac{(\sigma_1^2+\sigma_2^2-2|\sigma_1|\sigma_2\cosh\kappa h)}{(2\sinh\kappa h)^2}, \tag{2}$$

with ε the dielectric constant of water, and

$$\kappa^2=\frac{8\pi e^2}{\varepsilon k_B T}c \tag{3}$$

the Debye parameter. In Fig. 2 we show the curve $P(h)$. Attraction corresponds to $P(h)<0$ and repulsion to $P(h)>0$. The repulsion for small h values is caused by the effects of *counterion confinement* for $\sigma_2\neq|\sigma_1|$, we must maintain enough ions inside the gap in order to ensure local charge neutrality. As we reduce h, the osmotic pressure of the confined ions grows as $k_BT|\sigma_2+\sigma_1|/(eh)$, providing a repulsive pressure which competes with the electrostatic attraction. There thus exists an *equilibrium spacing* l^* with $P(h=l^*)=0$, which vanishes only when $\sigma_2=-\sigma_1$. It is well known that Eq. (2) incorporates some serious approximations. More accurate methods show that Eq. (2) is only valid

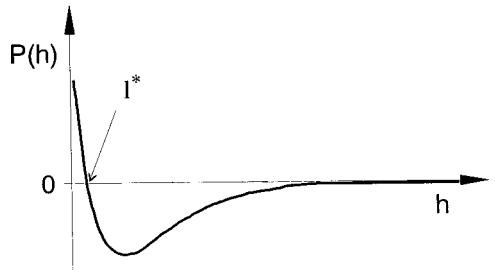

FIG. 2. Electrostatic force $P(h)$ per unit area as a function of the distance h between two membranes, bearing charge densities σ_1 and σ_2 of different sign and magnitude, given by Eq. (2). For $h>1^*$, the potential is attractive $[P(h)<0]$, whereas for $h<1^*$, the potential is repulsive $[P(h)>0]$, due to the increase of osmotic pressure of the confined counterions with reduction of h. In the case of different charge densities ($|\sigma_1|\neq\sigma_2$), ions are always trapped in the gap in order to ensure local charge neutrality and the equilibrium spacing l^* vanishes only when $\sigma_1=-\sigma_2$.

for larger h spacings [14]. Even then, the charge densities should be considered only as effective quantities.

Within the limitations of the DH theory, the work W performed by the electrostatic interaction as we bring the two membranes from infinity down to l^* is then computed as

$$W=-\int_{l^*}^{\infty}dh\ P(h). \tag{4}$$

After a straightforward calculation using Eq. (2) in Eq. (4), we find the following simple result:

$$W=\frac{4\pi}{\varepsilon\kappa}\begin{cases}\sigma_2^2, & \sigma_2<|\sigma_1|\\ \sigma_1^2, & \sigma_2>|\sigma_1|.\end{cases} \tag{5}$$

Note that there is a *mathematical singularity* at $\sigma_2=|\sigma_1|$.

The total free energy per unit area, $f(\sigma_1;\sigma_2)$, for the pair of membranes is now

$$f(\sigma_1;\sigma_2)\cong\sum_{i=1,2}\left\{\frac{k_BT}{e}|\sigma_i|[\ln(\sigma_i a_0/e)-1]+\frac{2\pi\sigma_i^2}{\varepsilon\kappa}\right\}-W. \tag{6}$$

The first term on the right hand side of Eq. (6) represents the free energy of isolated, charged membranes (i.e., with $h\to\infty$). It is the sum of an ideal mixing free energy for the charged lipids inside the membranes (with a_0 the area per lipid) plus the electrostatic self-energy of an isolated membrane, computed using the Debye-Hückel limit of the Poisson-Boltzmann free energy. The third term is the work of adhesion.

Equation (2) leads to the rather surprising prediction that two oppositely charged plates cannot properly adhere to each other unless we exactly match the surface charge densities. Osmotic pressure by confined counter ions in general prevents tight adhesion unless $\sigma_2=-\sigma_1$. To check whether these predictions of the equilibrium thermodynamics are indeed reliable, we still must require *thermodynamic stability*.

Since we are assuming that σ_1 is fixed, we only have to check the thermodynamic stability with respect to σ_2. Stability is obtained provided $\partial^2 f/\partial\sigma_2^2>0$. Using Eq. (6) we find that this requires that either $\sigma_2>|\sigma_1|$ or that $\sigma_2<\sigma^*$, with σ^* a threshold surface charge density given by

$$\sigma^*=\frac{\varepsilon\kappa k_BT}{4\pi e}. \tag{7}$$

Suppose we increase the fixed charge σ_1 starting from zero. We then first encounter a thermodynamically stable regime in the interval $0<|\sigma_1|<\sigma_2^0$ (with σ_2^0 the, initially uniform, cationic surface charge density). If $|\sigma_1|$ exceeds σ_2^0, then the σ_2 moiety will start to decompose provided $\sigma_2^0>\sigma^*$. Following the usual arguments on phase decomposition, we must expect the σ_2 membrane to decompose into two phases. One with $\sigma_2=|\sigma_1|$—which we will call the ''charge-regulated'' state—and a phase with $\sigma_2=\sigma^*$. The decomposition process can be illustrated by plotting $f(\sigma_2)$ as a function of σ_2 for fixed σ_1, using Eq. (6), where the hatched region in Fig. 3 is unstable. Note the cusp in the free energy at the charge-regulated state.

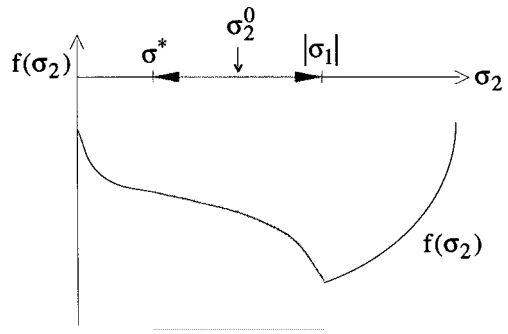

FIG. 3. $f(\sigma_2)$ as a function of σ_2 for fixed σ_1. The hatched region, limited by σ^* and $|\sigma_1|$, is unstable, which leads to a decomposition of the σ_2 (cationic) membrane into a ''charge-regulated'' phase with $\sigma_2=|\sigma_1|$ and a phase with $\sigma_2=\sigma^*$. σ_2^0 is the initially uniform charge density of the cationic membrane.

As noted earlier, if ion-dissociation rates are allowed to depend on the electrostatic potential, then charge regulation also can be achieved without phase separation [11,12]. Which of the two routes is chosen will depend on which form of charge regulation leads to the most significant lowering of the free energy. We will not carry out such a comparison theoretically, but allow on the analysis of the experiments described below.

We now apply this formalism to examine the adhesion of a cationic vesicle to an anionic surface with a fixed surface charge σ_1. We will assume the geometry of Fig. 4: σ_2^+ is the cationic lipid density of the adhesion disk of the vesicle, and σ_2^- is the density of the exterior section of the vesicle. The vesicle-substrate contact angle is ϑ_c, which is related to the radius R of the adhesion disk by $\sin\vartheta_c=R/r$, with r the vesicle radius. The adhesion induced vesicle tension is γ. It is a central claim of this paper that we are *not* permitted to involve the Young-Dupré law [Eq. (1), with $S=W$] to find the equilibrium value of ϑ_c. Instead, we will determine the equilibrium state by treating the edge of the adhesion disk as

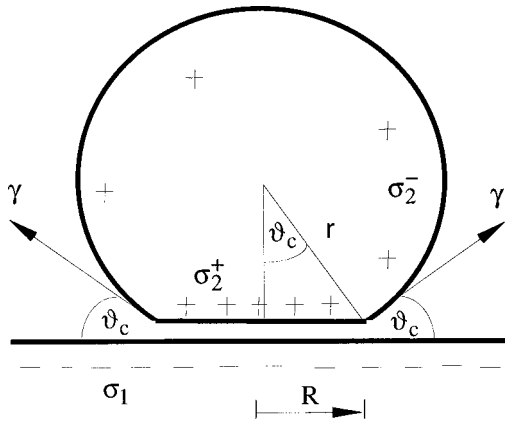

FIG. 4. Schematic drawing of a positively charged (+) vesicle, adhering to a negatively charged (−) substrate. σ_2^+ is the cationic lipid concentration in the adhesion disk, σ_2^- the cationic lipid concentration in the exterior section of the vesicle. σ_1 is the charge density of the substrate, R the radius of the adhesion disk of the vesicle, ϑ_c the contact angle between the vesicle membrane and the substrate, and γ the adhesion induced tension in the vesicle membrane. $|\sigma_2/\sigma_1|\ll 1$.

the boundary between two phases in contact (the adhesion disk and the vesicle exterior) which are in chemical equilibrium with each other. In addition, we also will require that the phase boundary is in osmomechanical equilibrium. The first condition is obtained if the chemical potential $\mu_2=e\partial f/\partial\sigma_2$ of the two phases is the same. Using Eq. (6) we find, for the chemical potentials,

$$\mu_2^{\pm}=k_BT\,\ln(\sigma_2^{\pm}/\sigma_0)\mp\frac{4\pi}{\varepsilon\kappa}\,\sigma_2^{\pm} \tag{8a}$$

for the case $\sigma_2^+<|\sigma_1|$, and

$$\mu_2^{\pm}=k_BT\,\ln(\sigma_2^{\pm}/\sigma_0)+\frac{4\pi}{\varepsilon\kappa}\,\sigma_2^{\pm} \tag{8b}$$

for the case $\sigma_2^+>|\sigma_1|$, with $\sigma_0=e/a_0$. Here, μ_2^+ and μ_2^- are, respectively, the chemical potential of the cationic lipids of the adhesion disk and of the vesicle exterior. Note that the disk chemical potential μ_2^+ undergoes a *jump* at $\sigma_2^+=|\sigma_1|$, which is due to the cusp singularity of the free energy at the charge-regulated state. Precisely at the charge-regulated state, the σ_2^+ chemical potential μ_2^+ actually can assume a *range* of values due to this cusp singularity:

$$k_BT\,\ln\left(\frac{\sigma 1}{\sigma_0}\right)-\frac{4\pi|\sigma_1|}{\varepsilon\kappa}\leqslant\mu_2^+\leqslant k_bT\,\ln\left(\frac{\sigma_1}{\sigma_0}\right)+\frac{4\pi|\sigma_1|}{\varepsilon\kappa}. \tag{9}$$

This has interesting consequences. Suppose we again increase σ_1 from zero. For $|\sigma_1|<\sigma_2^0$, with σ_2^0 the initial cationic vesicle lipid density, the condition $\mu_2^+=\mu_2^-$ simply reduces to $\sigma_2^+=\sigma_2^-=\sigma_2^0$: The cationic lipid density of the adhesion disk and vesicle are exactly the same. If we now increase $|\sigma_1|$ beyond σ_2^0, then σ_2^+ stays ''pinned'' at $|\sigma_1|$, since μ_2^+ can assume a wide range of values to match μ_2^-. For simplicity assume that the vesicle exterior acts like a *reservoir* for σ_2. In that case, $\sigma_2^-\cong\sigma_2^0$ (the initial cationic surface charge density of the vesicle). The chemical potential $\mu_2^+=\mu_2^-=\mu_2$ is then fixed by the reservoir at

$$\mu_2\cong k_BT\,\ln\left(\frac{\sigma_2^0}{\sigma_0}\right)+\frac{4\pi}{\varepsilon\kappa}\,\sigma_2^0. \tag{10}$$

As we increase $|\sigma_1|$ beyond σ_2^0, μ_2 remains inside the range given by Eq. (9), and σ_2^+ stays pinned at $|\sigma_1|$.

To impose osmomechanical equilibrium on the adhesion disk, we must require that the difference in two dimensional (2D) osmotic pressure across the phase boundary is equal to the externally applied 2D pressure by the vesicle tension by the principle of virtual work:

$$\pi^{(2)}(\sigma_2^+)-\pi^{(2)}(\sigma_2^-)=\gamma(1-\cos\,\vartheta_c). \tag{11}$$

Comparing Eqs. (1) and (11), we see that the spreading pressure S can be identified as $\pi^{(2)}(\sigma_2^+)-\pi^{(2)}(\sigma_2^-)$. This is the analog of the conventional Young's construction for membranes. Alternatively it can be also considered as the 2D analog of the standard requirement of osmomechanical equi-

librium for semipermeable membranes where we equate the osmotic pressure difference with the hydrostatic pressure difference.

The 2D osmotic pressure $\pi^{(2)}$ does *not* obey van't Hoff's law, as could have been guessed. It must be deduced from the definition of the osmotic pressure: $\pi^{(2)}(\sigma_2) = \sigma_2 df/d\sigma_2 - f(\sigma_2)$. If the cationic lipid density of the adhesion disk is less than that of the supported anionic membrane, i.e., if $\sigma_2^+ < |\sigma_1|$, then Eqs. (5) and (6) give the following free energy area density $f(\sigma_2^+)$ for the adhesion disk:

$$f(\sigma_2^+) \cong \frac{k_B T}{e}\,\sigma_2^+[\ln(\sigma_2^+ a_o/e) - 1] - \frac{2\pi(\sigma_2^+)^2}{\varepsilon\kappa} + C, \tag{12a}$$

where we only display the dependence of the free energy density on the σ_2 moiety [so the constant C in Eq. (12a) depends on σ_1]. The corresponding osmotic pressure is

$$\pi^{(2)}(\sigma_2^+) = k_B T\left(\frac{\sigma_2^+}{e}\right) - \frac{2\pi(\sigma_2^+)^2}{\varepsilon\kappa} - C, \quad \sigma_2^+ < |\sigma_1|. \tag{12b}$$

Note that the osmotic pressure has been lowered compared to van't Hoff's law due to the electrostatic interaction. If we view Eq. (12b) as a virial expansion, then the second virial coefficient is negative and equal to $B = -2\pi/\varepsilon\kappa$. The electrostatic interaction thus has destabilized the adhesion disk in this regime. On the other hand, if the cationic lipid density of the adhesion disk exceeds that of the supported anionic membrane, then Eqs. (5) and (6) give

$$f(\sigma_2^+) \cong \frac{k_B T}{e}\,\sigma_2^+[\ln(\sigma_2^+ a_o/e) - 1] + \frac{2\pi(\sigma_2^+)^2}{\varepsilon\kappa} - \frac{4\pi(\sigma_1)^2}{\varepsilon\kappa} + C, \tag{12c}$$

with the constant C the same as in Eq. (12a). The corresponding osmotic pressure is

$$\pi^{(2)}(\sigma_2^+) = k_B T\left(\frac{\sigma_2^+}{e}\right) + \frac{2\pi(\sigma_2^+)^2}{\varepsilon\kappa} + \frac{4\pi(\sigma_1)^2}{\varepsilon\kappa} - C, \quad \sigma_2^+ > |\sigma_1|. \tag{12d}$$

The second virial coefficient is now positive, so, for $\sigma_2^+ > |\sigma_1|$, electrostatics stabilizes the adhesion disk. Note that there is a jump in the osmotic pressure at $\sigma_2^+ = |\sigma_1|$. Finally, for the cationic lipid density outside the adhesion disk, we must set $W = 0$ in Eq. (6), and we find, over the whole range, a positive second virial coefficient:

$$\pi^{(2)}(\sigma_2^-) = k_B T\left(\frac{\sigma_2^-}{e}\right) + \frac{2\pi(\sigma_2^-)^2}{\varepsilon\kappa} - C. \tag{12e}$$

Once again, we increase σ_1 from zero. In the stable interval $0 < |\sigma_1| < \sigma_2^0$, we found that $\sigma_2^+ = \sigma_2^- = \sigma_2^0$. Using Eqs. (12d) and (12e) in Eq. (11) gives $S = \gamma(1 - \cos\vartheta_c)$, with a spreading pressure

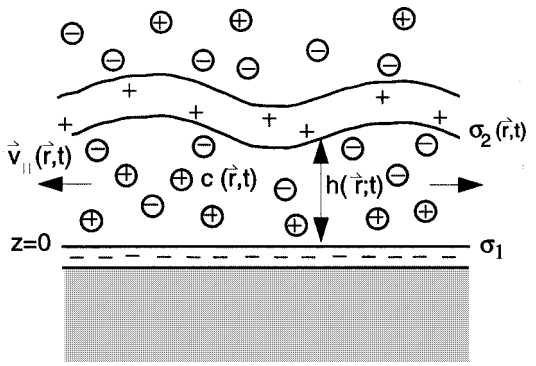

FIG. 5. Scenario of two adjacent, oppositely charged, membranes. The supported membrane at $z = 0$ is assumed to have fixed surface charges (charge density σ_1), and to be impermeable to both water and salt ions. The minority charged membrane surface charge density $\sigma_2(\vec{r};t)$ is assumed to be permeable to water but not to salt ions. $\vec{r}$ is a coordinate in the plane of the supported membrane. $v_\parallel(\vec{r};t)$ denotes the flow field parallel to the supported membrane, $c(\vec{r};t)$ the ion concentration in the gap between the two membranes, and $h(\vec{r};t)$ their distance.

$$S = \frac{4\pi}{\varepsilon\kappa}\,\sigma_1^2, \quad |\sigma_1| < \sigma_2^0, \tag{13a}$$

which is equal to the specific adhesion energy W for $|\sigma_1| < \sigma_2$ according to Eq. (5). For $|\sigma_1| > \sigma_2^0$, we can set $\sigma_2^+ = |\sigma_1|$ and $\sigma_2^- \cong \sigma_2^0$. *Under these conditions, we find a spreading pressure*

$$S = W - \frac{2\pi}{\varepsilon\kappa}\,(|\sigma_1| - \sigma_2^0)^2 + k_B T\,\frac{|\sigma_1|}{e}\ln\left(\frac{\sigma_2^0}{|\sigma_1|}\right) + \frac{k_B T}{e}\,(|\sigma_1| - \sigma_2^0), \quad |\sigma_1| > \sigma_2^0, \tag{13b}$$

that is not equal to W. We again treated the vesicle exterior as a reservoir. This expression can only be valid for $|\sigma_1|$ comparable to σ_2^0, since, for $|\sigma_1| \gg \sigma_2^0$, the vesicle exterior will be depleted in anionic lipids and no longer can act as reservoir. The specific adhesion energy $W = 4\pi\sigma_1^2/(\varepsilon\kappa)$ in Eq. (13b) is that of the charge-regulated state of the adhesion disk $\sigma_2^+ = |\sigma_1|$ computed at a fixed concentration. Comparing Eqs. (13a) and (13b), we see that $|\sigma_1| = \sigma_2^0$ marks the onset of breakdown of Young-Dupré relation. For $|\sigma_1| > \sigma_2^0$, the spreading pressure S is in general *less* than the work of adhesion due to the reorganization of the lipids in the adhesion disk.

B. Adhesion kinetics

To examine the kinetics of the adhesion process, we will use a simplified set of hydrodynamic equations of motion for the conserved fields in our problem: the salt concentration $c(\vec{r};t)$, the minority surface charge density $\sigma_2(\vec{r};t)$, and the flow field $\vec{v} = [v_z(\vec{r};t), v_\parallel(\vec{r};t)]$, with $\vec{r}$ a direction vector in the plane of the membrane (Fig. 5). We will assume that the majority-charged membrane at $z = 0$ has a fixed surface charge density σ_1, and that it is impermeable to both water and salt ions (see also Fig. 1). The σ_2 minority-charged membrane at $z = h(\vec{r};t)$ is assumed to be permeable to water

but *not* to salt ions. The permeability for water will be denoted by λ. Both membranes are assumed to be circular with a radius R. At time $t=0$, the majority surface charge density σ_1 is upregulated from zero to a finite value $|\sigma_1| \gg \sigma_2$ with $\sigma_1<0$ and $\sigma_2>0$, as before.

The hydrodynamic equations we will use are

$$\frac{\partial c}{\partial t}+\vec{v}_{\|}\cdot\vec{\nabla}c+\frac{c}{h}\frac{\partial h}{\partial t}=D_s\nabla^2 c, \tag{14}$$

$$\frac{\partial \sigma_2}{\partial t}=\frac{D_{\sigma_2}}{k_B T}\vec{\nabla}\cdot(\sigma_2\vec{\nabla}\mu_{\sigma_2}), \tag{15}$$

$$\eta\nabla^2\vec{v}=\vec{\nabla}P. \tag{16}$$

Equation (14) is the advection-diffusion equation, with D_s the diffusion constant of the salt (we neglect variation of c in the z direction). The origin of the term $(c/h)\partial h/\partial t$ in Eq. (14) is understood by noting that, in the absence of diffusion and flow, the product ch must remain constant: if h decreases—by solvent permeation—then c must increase as $1/h$ due to the impermeability of the membranes for the salt ions. In that case, $\partial c/\partial t=-c/h\,\partial h/\partial t$. Adding transport by advection and diffusion gives Eq. (14). Equation (15) is the diffusion equation (in two dimensions) for the minority-charged surfactant molecules, with D_{σ_2} the diffusion constant. The chemical potential

$$\mu_{\sigma_2}=e\frac{\partial}{\partial\sigma_2}f(\sigma_1,\sigma_2) \tag{17}$$

is found from Eq. (6), but where we now allow h to differ from l^*,

$$\mu_{\sigma_2}\cong k_B T\ln\left(\frac{\sigma_2}{e}a_o\right)+\frac{4\pi e\sigma_2}{\varepsilon\kappa}-\frac{8\pi e|\sigma_1|}{\varepsilon\kappa}e^{-\kappa h}, \tag{18}$$

assuming $\kappa h\gg 1$. Finally, Eq. (16) is the equation of motion for the solvent fluid in the Stokes approximation, with η the viscosity. The boundary conditions for the solution of Eq. (16) are

$$\vec{v}|_{z=0}=0, \tag{19}$$

which expresses the impermeable nature of the $z=0$ surface, and

$$\frac{\partial h}{\partial t}-v_z|_{z=h}=\lambda\{P(h)+k_B T(c-c_0)\}, \tag{20a}$$

$$\vec{v}_{\|}|_{z=h}=0. \tag{20b}$$

Equation (20a) describes permeative transport through the membrane. The second term inside the brackets is the excess osmotic pressure due to salt ions trapped between the membranes, with c_0 the salt concentration of the surrounding reservoir. Equation (20b) states that we do not allow flow inside the membrane. In the following we will discuss the hydrodynamics, using only qualitative methods aimed at providing physical insight into the adhesion process.

1. Uniform relaxation

We start by assuming that σ_2 and h are independent of $\vec{r}$, and study how $h(t)$ depends on time following upregulation of σ_1 at $t=0$. The initial value $h_0=h(t=0)$ is assumed to be large compared to the new equilibrium spacing $l^*\cong\kappa^{-1}\ln(|\sigma_1/\sigma_2|)$ [found by setting $P(h)=0$ in Eq. (2)]. The relaxation of h from h_0 to l^* follows a two time scale scenario. First, h can relax rapidly via solvent permeation to a state of local mechanical equilibrium. By this we mean that the electrostatic and osmotic pressures on the minority charged membrane are in balance. If $\bar{h}$ and $\bar{c}$ are, respectively, the spacing and salt concentration of this state, then

$$P(\bar{h})+k_B T(\bar{c}-c_0)\approx 0. \tag{21}$$

This is a *nonconserved* process requiring a relaxation time τ_1 of order

$$\tau_1\approx 1\Big/\left(\lambda\frac{\partial P}{\partial h}\right), \tag{22}$$

which is independent of the disk radius R (see Fig. 4). Since we do not allow flow or diffusion to contribute to permeative relaxation, ch must be constant, so $\bar{c}=c_1$ with $c_1=c_0h_0/\bar{h}$.

The second type of relaxation involves diffusion and flow, which are slower, conserved processes. Solute diffusion from the region of the gap to the surrounding fluid is driven by the concentration gradient $(\bar{c}-c_0)/R$. Similarly, hydrodynamic flow from the gap region to the ambient fluid is driven by the hydrodynamic pressure gradient $[-P(\bar{h})]/R$ (setting the pressure in the ambient fluid to zero). Both processes allow excess salt ions to escape from the gap regions. The time scale for diffusive relaxation τ_2^D is

$$\tau_2^D\propto(1/D_s)R^2, \tag{23}$$

while, for hydrodynamic relaxation,

$$\tau_2^H\propto\left(\frac{\eta}{\bar{h}^2|P(\bar{h})|}\right)R^2, \tag{24}$$

using the classical result of Reynolds on flow from between two plates pressed together by an external force. We will assume the disk radius R to be sufficiently large so $\tau_1\ll\tau_2^{D,H}$, which implies that the membrane remains in local mechanical equilibrium during the relaxation process.

It is helpful to illustrate the two step relaxation process in a qualitative manner, for the case that the τ_2 process is due to diffusion. Suppose we start at $t=0$ with $h=h_0$. After upregulation of $|\sigma_1|$, the new quasiequilibrium state with $h=h_1$ is found from Eq. (21):

$$P(h_1)+k_B Tc_0\left(\frac{h_0}{h_1}-1\right)=0. \tag{25}$$

We can construct h_1 graphically from the intersection of $P(h)$ with the curve $k_B Tc_0(1-h_0/h)$ [Fig. 6(a)]. The excess osmotic pressure inside the gap is now $\Delta\pi_1=k_B Tc_0(h_o/h_1)$. Next we keep h fixed at h_1, and allow diffusion to remove the excess salt from between the membranes, requiring a time $\tau_2\propto R^2/D$. As a result the membrane

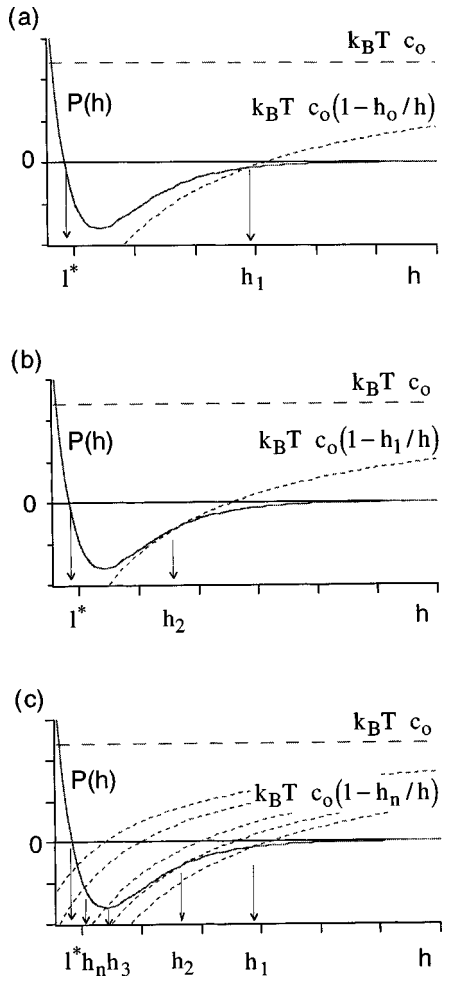

FIG. 6. Illustration of the relaxation process of the spacing h between two membranes with $\sigma_1<0$ and $\sigma_2>0$ to the new equilibrium spacing l^* after a jumpwise increase of $|\sigma_1|$. Immediately after upregulation of $|\sigma_1|$, the distance h between the two membranes is reduced from h_0 to h_1. $P(h_1)$ is counterbalanced by the excess osmotic pressure inside the gap, $\Delta\pi_1=k_BTc_0h_0/h_1$. This quasiequilibrium state can be constructed graphically from the intersection of $P(h)$ with $k_BTc_0(1-h_0/h)$ (a). After diffusion of the excess ions out of the gap the spacing, h is further reduced to the quasiequilibrium state with $h=h_2$, which is found graphically from the intersection of $P(h)$ with $k_BTc_0(1-h_1/h)$ (b). Repeating this graphical construction gives a succession of spacings $h_n=h_1,h_2,h_3,\ldots$, which approximate the equilibrium state $h=l^*$ for large n (c).

is out of mechanical equilibrium. The new mechanical equilibrium state h_2 is found by constructing the intersection of $P(h)$ with $k_BTc_0(1-h_1/h)$ [Fig. 6(b)], producing a new excess osmotic pressure $\Delta\pi_2=k_BTc_0(h_1/h_2)$. Repeating this graphical construction gives a succession of spacings $h_n=h_1,h_2,h_3,\ldots$, which approximate the equilibrium state $h=l^*$ for large n [Fig. 6(c)]. Note that the excess osmotic pressure first increases and then drops.

2. Linear-response theory

To examine the stability of this uniform relaxation process against small perturbations, we expand

$$c(\vec{r},t)=\overline{c}+c'(\vec{r},t), \tag{26a}$$

$$\sigma_2(\vec{r},t)=\overline{\sigma_2}+\sigma'(\vec{r},t), \tag{26b}$$

$$h(\vec{r},t)=\overline{h}+h'(\vec{r},t), \tag{26c}$$

with $c'/\overline{c}$, $\sigma'/\overline{\sigma_2}$ and $h'/\overline{h}$ infinitesimal.

We insert Eq. (26) into the hydrodynamic equations under the following assumptions: (i) no hydrodynamic flow, and (ii) local mechanical equilibrium [so Eq. (21) also remains valid for the perturbed fields]. We will include effects (i) and (ii) below. After linearization we find

$$\frac{\partial c'}{\partial t}+\left(\frac{\overline{c}}{\overline{h}}\right)\frac{\partial c'}{\partial t}=D_s\nabla^2c', \tag{27a}$$

$$\frac{\partial\sigma'}{\partial t}=D^e_{\sigma_2}\nabla^2\sigma'+e\Delta cD_{\sigma_2}\nabla^2h', \tag{27b}$$

$$\left.\frac{\partial P}{\partial h}\right|_{\overline{h}}h'+\left.\frac{\partial P}{\partial\sigma_2}\right|_{\overline{\sigma_2}}\sigma_2'+k_BTc'=0. \tag{27c}$$

Here

$$D^e_{\sigma_2}=D_{\sigma_2}\left(1+\frac{4\pi e\overline{\sigma_2}}{\varepsilon k_BT\kappa}\right) \tag{28}$$

is the effective single-layer surface diffusion constant (i.e., including electrostatic self-energy effects) while the constant

$$\Delta c\equiv\frac{8\pi|\sigma_1|\overline{\sigma_2}}{\varepsilon k_BT}\,e^{-\kappa\overline{h}} \tag{29}$$

has units of concentration. The average values $\overline{c}$ and $\overline{h}$ here are actually time dependent, as discussed in Sec. II B 1, but always connected through the condition of local mechanical equilibrium, Eq. (21). Using Eq. (2) with $\sigma_2\ll|\sigma_1|$ in Eq. (21) allows us to simplify Eq. (27c) to

$$\left[\frac{2(\overline{c}-c_0)-\Delta c}{c_0}\right](\kappa h')-\left(\frac{\Delta c}{c_0}\right)\left(\frac{\sigma_2'}{\overline{\sigma_2}}\right)+\left(\frac{c'}{c_0}\right)=0. \tag{30}$$

We look for solutions to Eq. (27) of the forms

$$c'(\vec{r},t)=c_qe^{-\omega_qt+i\vec{q}\cdot\vec{r}}, \tag{31a}$$

$$\sigma'(\vec{r},t)=\sigma_qe^{-\omega_qt+i\vec{q}\cdot\vec{r}}, \tag{31b}$$

$$h'(\vec{r},t)=h_qe^{-\omega_qt+i\vec{q}\cdot\vec{r}}. \tag{31c}$$

Stability requires that only solutions with $\omega_q>0$ exist. Inserting Eq. (31) into Eq. (27) leads to

$$(-\omega_q+D_sq^2)c_q-\omega_q\left(\frac{\overline{c}}{\overline{h}}\right)h_q=0, \tag{32a}$$

$$(-\omega_q+D^e_sq^2)\sigma_q+e\Delta cD_{\sigma_2}q^2h_q=0, \tag{32b}$$

$$\Gamma(\kappa h_q)-\frac{\Delta c}{c_0}\left(\frac{\sigma_q}{\overline{\sigma_2}}\right)+\frac{c_q}{c_0}=0, \tag{32c}$$

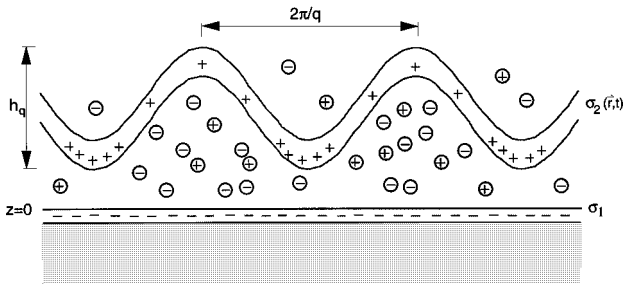

FIG. 7. Decomposition process of the minority charged membrane. The supported membrane at $z=0$ bears a homogeneous majority charge density σ_1. The fluid minority charged (σ_2) membrane decomposes into patches of enriched charge density (with $\sigma_2=-\sigma_1$) and into regions of reduced charge density (with $\sigma_2=\sigma^*$), where the solutes are enriched and trapped between the membranes. $2\pi/q$ characterizes the wavelengths of the unstable undulation modes of height h_q.

with $\Gamma=[2(\bar{c}-c_0)-\Delta c]/c_0$. The onset of instability is marked by the appearance of solutions to Eq. (32) with $\omega_q=0$. Such solutions appear when

$$\Gamma\kappa+\frac{e\Delta c^2}{c_0}\left(\frac{D_{\sigma_2}}{D^e_{\sigma_2}}\right)=0. \tag{33}$$

This condition can be simplified using Eqs. (4), (9), (28), and (29). Define a critical spacing

$$h_c=l^*+\frac{1}{\kappa}\ln\left(\frac{2\sigma^*}{\sigma_2+\sigma^*}\right). \tag{34}$$

For $\bar{h}>h_c$ only positive ω_q solutions exist, while an unstable mode appears for $\bar{h}<h_c$. The quantity σ^* in Eq. (34) is just the σ_2 stability threshold encountered in Sec. II A. The unstable mode for $\bar{h}<h_c$ has a q^2 spectrum,

$$\omega(q)\cong-D_{\sigma_2}\left(\frac{h_c-\bar{h}}{h_c}\right)q^2. \tag{35}$$

Note that the instability only can appear if h_c is greater than l^*—the equilibrium spacing. This condition is equivalent to demanding that σ_2 must exceed σ^*. We thus recover the result of equilibrium theory that $\sigma_2=\sigma^*$ is the stability limit. The structure of the marginally stable mode, with $\omega(q)=0$, follows from Eq. (32),

$$\sigma_q=-e\Delta c\left(\frac{D_{\sigma_2}}{D^e_{\sigma}}\right)h_q, \tag{36}$$

while $c_q=0$. The concentration fluctuation is thus out of phase with the height fluctuation. As shown in Fig. 7, this means that the regions of excess charged surfactant are close to the (oppositely charged) support, while regions depleted in charged surfactant are moved further away. Note that, even though $c_q=0$, there are more trapped salt ions in the charge-depleted regions than in the charge-enriched regions.

In the preceding analysis we neglected deviations from local mechanical equilibrium—which involve permeation [see Eq. 20(a)] and hydrodynamic flow. Both effects lead to relaxation. The relaxation rate ω^R of a deformed membrane

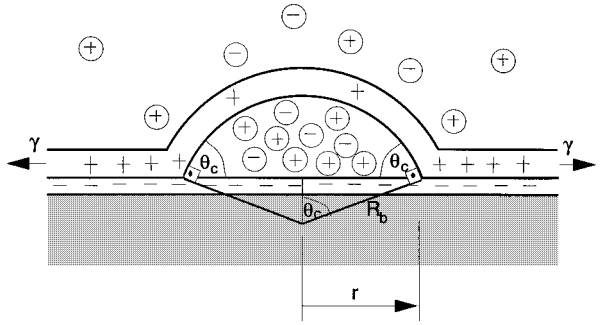

FIG. 8. Late stage of membrane decomposition. At the patches of enriched charge density ($\sigma_2=-\sigma_1$) the membranes are in close contact. Solutes are enriched and trapped in the gap between the two membranes at the areas of depleted charge density ($\sigma_2=\sigma^*$). This causes osmotic pressurized ''salt bubbles,'' which form spherical caps of radius R_b. r is the radius of the disk of the bubble, ϑ_c the contact angle, measured at the intersection of the bubble membrane with the supported membrane, and γ the adhesion-induced tension of the minority charged membrane.

by permeation and flow in proximity of a flat surface at a distance h was computed—for a similar set of hydrodynamic equations—by Lennon and Brochard [15], with the result

$$\omega^R=\lambda K_c q^4+\frac{h_c^3}{12\eta}K_c q^6, \tag{37}$$

with K_c the Helfrich bending modulus of the membrane. The complete spectrum of the unstable mode near $\bar{h}=h_c$ is then

$$\omega(q)\cong-\alpha D_{\sigma_2}\left(\frac{h_c-\bar{h}}{h_c}\right)q^2+\lambda K_c q^4+\frac{h_c^3}{12\eta}K_c q^6, \tag{38}$$

with α a numerical constant. The wave vector q^* of the unstable mode for h_c close to $\bar{h}$ is thus

$$q^*\propto\left[\frac{D_{\sigma_2}}{\lambda K_c}\left(\frac{h_c-\bar{h}}{h_c}\right)\right]^{1/2}. \tag{39}$$

3. Late-stage decomposition

The later stages of the membrane decomposition process can be inferred from the nature of the unstable mode (see Fig. 8) and our earlier discussion. Those parts of the membrane which are enriched in positive charge will come into contact with the substrate. They are expected to have a surface charge density $\sigma_2=|\sigma_1|$, as follows from the discussion of the equilibrium adhesion energy.

The regions which are depleted in cationic surfactant material are prevented from adhering material to the substrate by the added solute trapped between the membranes. We thus expect the formation of charge-regulated adhesion areas interspersed with a weak-adhesion area, with $\sigma_2\approx\sigma^*$ capturing excess salt. The initial size of these regions will be of order q^{*-1}. These salt bubbles, or ''blisters,'' as we will call them, should be pressurized due to the osmotic pressure of the excess salt. The excess hydrostatic pressure should obey Laplace's law

$$\Delta P = \frac{2\gamma}{R_b}, \tag{40}$$

with R_b the curvature radius of the blister. The three-dimensional excess osmotic pressure $\Delta\pi^{(3)}$ of the blister should equal ΔP. The blister thus should have the shape of a hemispherical cap. The contact angle ϑ_c between the caps and the substrate should be determined by the same type of arguments which leads to Young's law

$$S = \gamma(1 - \cos\ \vartheta_c), \tag{41}$$

and we expect ϑ_c to be equal to the contact angle between the vesicle and substrate.

It follows from Eq. (40) that if a collection of salt blisters of various radii forms, then both the hydrostatic and osmotic pressures inside the blisters should be inversely proportional to R_b. This process should lead to *coarsening* phenomena: small blisters will be adsorbed by large blisters, leading to a growth of the mean size. If two blisters come into close contact, then the smaller blister must drain into the larger blister, either by hydrodynamic flow (driven by the difference in ΔP values) or by diffusion (driven by the difference in $\Delta\pi$ values). The mean blister size should grow with time. Similar phenomena are well known from studies of the evolution of foams [16].

III. EXPERIMENTAL TESTS AND DISCUSSION

A. Evolution of blistering

Figures 9(a) and 9(b) show typical RICM images of a cationic vesicle close to an anionic substrate at pH 2.8 and 4.5, respectively. The detailed description of the system and the preparation procedure are described in the Appendix. The vesicle contained 1 mol% of positively charged dihexadecyldimethyl ammonium bromide (DHDAB), and the supported membrane 10 mol% of negatively chargeable lipid octadecyl-[NBD-decyl]-dimethyl ammonium succinic acid (NBD-DODA-SA) [17]. The outer solution of the vesicle contained 5-mM sodium chloride (NaCl) and 10-mM sucrose and citric acid, which was isoosmolar to 30-mM sucrose. The inner solution contained 40-mM sucrose and 5-mM NaCl.

At pH 2.8 ($\sigma_1 \cong 0$), the vesicle exhibits a small and homogeneous adhesion disk, with a large number of diffraction fringes, indicating that the contact angel is small and that adhesion is weak [see Eq. (1)]. Weak adhesion is also suggested by the fact that pronounced flickering of the vesicle is observed, indicating a low vesicle tension γ. At pH 4.5 we find that the adhesion disk decomposes into blisters surrounded by regions of strong, close adhesion. Flickering is supressed, indicating that the vesicle is under appreciable tension.

The full scenario of blister formation is shown in Fig. 10(a) for the case of a change in pH from 4.1 to 4.5. According to separate experiments, a pH change is accomplished within about 20 min. The sequence of images shows that, during the increase of the adhesion area, blisters form spontaneously both within the adhesion disk and at the leading front of the spreading vesicle.

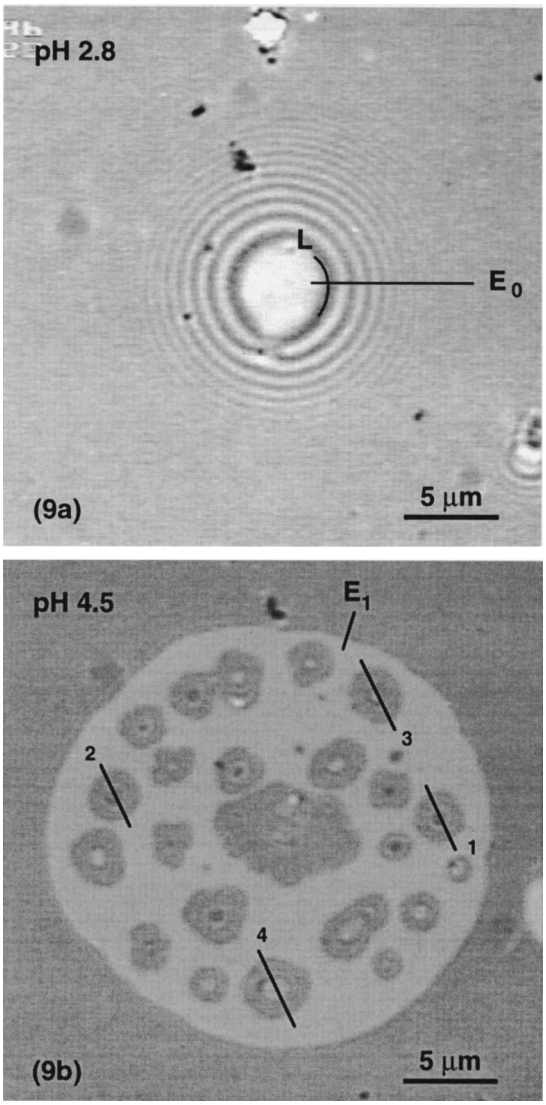

FIG. 9. Typical RICM image of a positively charged vesicle, which is electrostatically attracted to a negatively charged substrate, at pH 2.8 (a) and pH 4.5 (b). At pH 2.8 the vesicle exhibits a small homogeneous contact area, whereas at pH 4.5 the increased contact area shows a large number of domains, exhibiting two or three diffraction fringes. The vesicle contained 1 mol % of positively charged DHDAB, and the supported membrane 10 mol % of the negatively chargeable NBD-DODA-SA. The pH was adjusted from the initial 2.8 to 4.5, by incremental steps of 0.3 pH units. Simultaneously, the volume of the vesicle was reduced by a factor 0.22, as described in the Appendix. The dark lines mark the sections along which the surface profile was analyzed. Note that the blister in the center of contact area of (b) was induced by a small lipid particle trapped on the surface of the supported membrane. Within the resolution of RICM, no nucleating particles could be detected at the sites of the other blisters.

For a quantitative evaluation of the time evolution of blisters, the reduced area of blisters, α_b, and the reduced number of blisters, n_b, was determined. α_b is defined here as the ratio of the sum of the areas of the blisters to the total area of the contact zone. The membrane area of the blisters, A_b, is estimated from the blister radius in the contact zone, r, and the height h of the blister, according to $A_b = \pi r\sqrt{r^2 + h^2}$. The value of h was obtained by analyzing the RICM interfero-

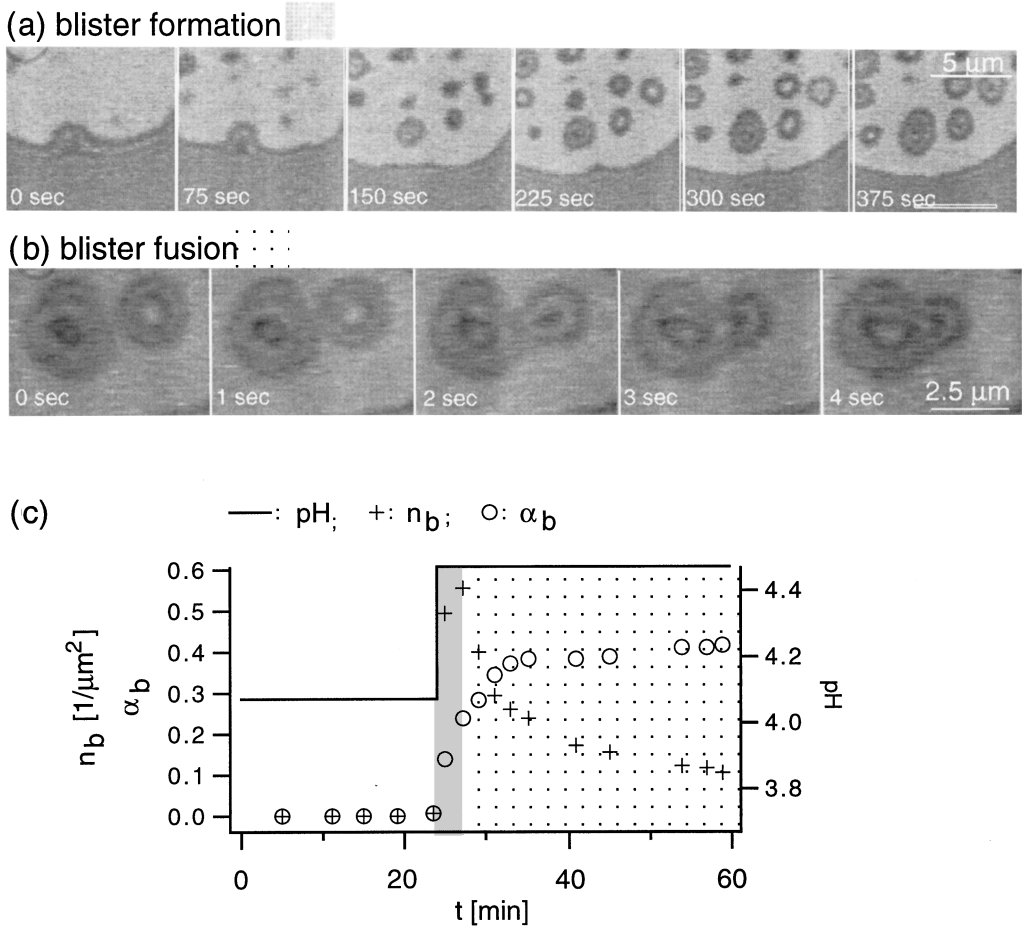

FIG. 10. (a) Scenario of blister formation during an increase of the contact area after an increase of the *p*H from 4.1 to 4.5. The frames were taken every 75 s. Note that blisters form both within the adhesion area and at the spreading front of the vesicle. (b) Demonstration of fusion of blisters 14 min after formation. The time interval between the frames is 1 s. (c) Plot of the time dependence of the reduced number of blisters (crosses) and the reduced contact area of blisters (circles) after increasing the *p*H from 4.1 to 4.5 inside the dialysis tubes (indicated by the steplike line). The pH inside the chamber is adjusted to the new value within 20 min, following an exponential function [J. Nardi (unpublished)].

grams. n_b is the actual number of the blisters divided by the total area of the blisters. As shown in Fig. 10(c), the reduced blister area, α_b (open circles) increases monotonically with time, and reaches saturation after 12 min. In contrast, the reduced number of blisters n_b increases sharply to a maximum, and decreases again with increasing time. The latter finding is a consequence of the fusion of the blisters, which is demonstrated in Fig. 10(b). A closer inspection of a number of fusion processes shows that smaller blisters always drained into larger blisters, as predicted by the theory. This fusion behavior of the pressurized blisters is indeed reminiscent of the fusion of interconnected soap bubbles. This described evolution of blisters may underly the blisterlike pattern, which has been observed in contact area of erythrocytes, which were agglutinated by polylysine [18].

B. Analysis of contour—measurement of spreading pressure

Following a procedure reported previously [19], the spreading pressure S, defined in Eq. (1), is determined by simultaneous measurement of the contact angle ϑ_c and the adhesion-induced membrane tension γ, based on the analysis of the contour of the membrane surface at the rim of the adhesion disk and of the blisters, respectively. An example of such an analysis for the outer rim of the vesicle is shown in Fig. 11(a) for the case of the weakly adhering state (*p*H 2.8). The vesicle contour is straight far from the contact line L, as should be expected for adhesion of a tense vesicle. Close to the contact line L the membrane is bent and goes smoothly over into the adhesion disk [20]. The slope of the tangent of the straight section defines an effective contact angle ϑ_c, which enters in Eq. (1). The distance λ between the intersection of this tangent with the horizontal axis and the contact line L defines a crossover length λ, which is related to the bending modulus K_c and the membrane tension γ by [21]

$$\lambda = \left(\frac{K_c}{\gamma}\right)^{1/2}. \tag{42}$$

The physical meaning of λ is that membrane deflections at length scales larger than λ are dominated by tension and deflections at scales smaller than λ by membrane bending rigidity. Since the bending modulus of the membrane can be measured in a separate experiment (e.g., by flicker spectroscopy [22]) the spreading pressure S now can be obtained by separately measuring λ and ϑ_c. In the following we will

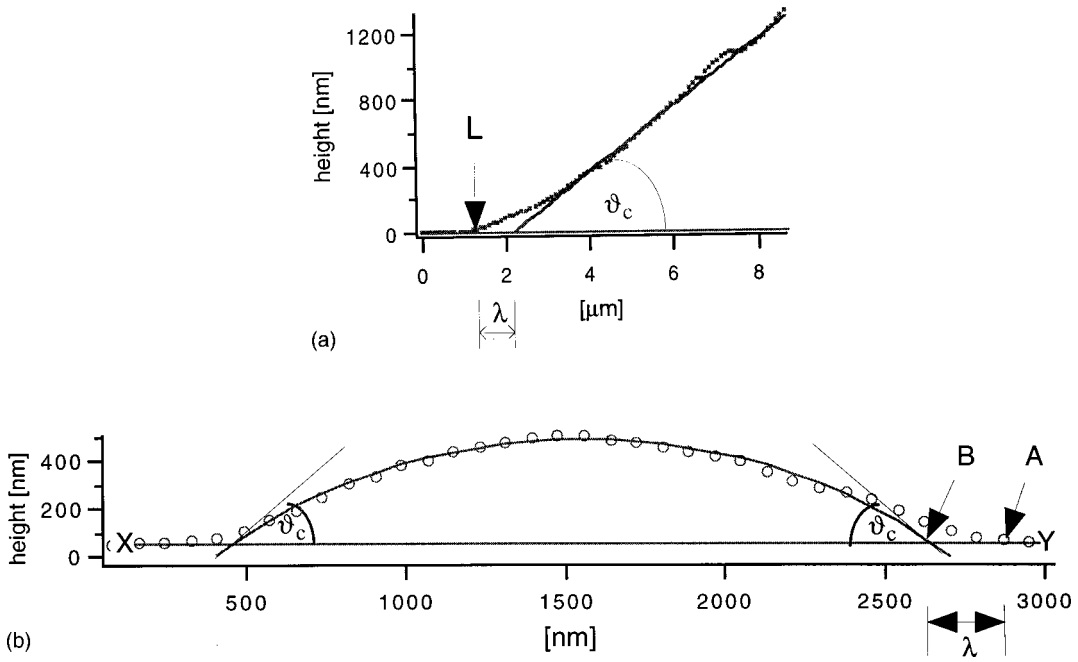

FIG. 11. (a) Contour of the vesicle near contact line L as obtained by analyzing the interference pattern of the RICM micrograph shown in Fig. 9(a) along line E_0, which is perpendicular to contact line L. The crossover length λ and contact angle ϑ_c are defined as shown graphically. (b) Reconstruction of the surface profile of a blister (circles) as obtained by analyzing the interference pattern of the RICM micrograph shown in Fig. 9(b) along line 1. Crossover length λ is defined by the distance *AB*. *A* is the point on the contact line L where the vesicle membrane starts to curve away from the substrate, and *B* is the intersection of the base line *XY* with the circle segment (radius R_b) fitted to the central part of the blister surface profile. The contact angle ϑ_c is the angle at the intersection of the base line *XY* and the tangent of the fitted circle at point *B*.

use for the value of K_c that of a 1:1 *L*-α-dimyristoylphosphatidylcholine (DMPC)-cholesterol mixture: $K_c = 10^{-18} J/m^2$ [23]. The values of S obtained in this manner by analyzing the contour at the rim of adhesion disk at pH 2.8 and 4.5 are given in Table I. For comparison we also present the calculated values of the specific adhesion energy per unit area, W, using Eq. (5). For pH 2.8, $\sigma_2 > |\sigma_1|$, and we can directly use Eq. (5) with $W = (4\pi)\sigma_1^2/(\varepsilon\kappa)$. For pH 4.5, where $|\sigma_1| > \sigma_2$, we are in the regime of charge regulation with $\sigma_2^+ = |\sigma_1|$. If we would compute the work of adhesion at a fixed surface charge $|\sigma_2| = |\sigma_1|$ we would again find $W = (4\pi)\sigma_1^2/(\varepsilon\kappa)$. If, on the other hand, we would let the mobile charges relax during the separation of the surfaces, then W would be reduced due to the electrostatic free energy cost of concentrating the charges in the adhesion disk and the corresponding entropic free energy cost. This leads to a similar adhesion energy $W = (2\pi)\sigma_1^2/(\varepsilon\kappa)$, which is reduced by one half. For the case of a vesicle containing 1 mol% of (positively) charged lipid, the cationic charge density is $\sigma_2 = 1.6 \times 10^{-3}$ C/m^2 (assuming an area per lipid of 100 Å^2). The charge density of the supported membrane at pH 2.8 is $\sigma_1 \approx -1.6 \times 10^{-5}$ C/m^2. [9]. The resulting ratio S/W of the spreading coefficient to the specific adhesion energy is then $S/W \approx 1.5$ for the case of weak adhesion, and $S/W \approx 10^{-3}$ for the case of tight adhesion.

TABLE I. Adhesion energy W and spreading coefficient S, as obtained by analysis of the contour of the adhered vesicle, at pH 2.8 along section E_0 [Fig. 9(a)] and pH 4,5 along section E_1 [Fig. 9(b)]. The last column gives the ratio of S/W.

pH	2.8	4.5
S (J/m^2)	4.5×10^{-8}	9×10^{-7}
W (J/m^2)	3×10^{-8}	1.5×10^{-4}
S/W	1.5	6×10^{-3}

Next, we performed a contour analysis of the blisters. Figure 11(b) shows a reconstruction of the surface profile (circles) along the section through the center of a blister at *p*H 4.5 [denoted by 1 in Fig. 9(b)]. By following the time evolution of the shape of the blisters from the onset of blister formation to the state shown in Fig. 9, we found that the shape always is that of a spherical cap in the center, but exhibiting a smoothly curved transition into the tight adhe-

TABLE II. Characteristic parameters of blisters 1–4 in Fig. 9(b). The parameters are radius R_b, contact angle ϑ_c, crossover length λ, adhesion-induced membrane tension γ, spreading coefficient S, Laplace pressure ΔP, and enriched concentration of ions Δc in the blister caps. For comparison, the corresponding values of the contour at the edge of adhesion disk along section E_1 are added.

Blister No.	1	2	3	4	E_1
R_b (μm)	1.6	1.6	2.0	2.4	
ϑ_c (°)	45	45	38	41	32
λ (nm)	360	470	447	466	465
γ (10^{-6} J/m^2)	7.0	4.5	5.0	5.0	4.5
S (10^{-6} J/m^2)	2.1	1.4	1.1	1.3	0.9
ΔP (N/m^2)	9	6	5	4	
Δc (10^{-6} M)	3.6	2.4	2.0	1.6	

sion area. The blister size (bottom diameter and height) increases both with pH and with time. For evaluation of blisters in terms of the crossover length λ and contact angle ϑ_c, the following procedure was applied. A circular segment of radius R_b was fitted to the central part of the reconstructed blister cap. The contact angle ϑ_c was determined as the angle of intersection of the base line (denoted as X-Y) and the fitted cap [Fig. 11(b)]. The crossover length λ was the distance between this point of intersection (denoted as B) and the point where the membrane starts to curve away from the base line (denoted as A).

In Table II, the results are given for a number of analyzed blisters [denoted in Fig. 9(b) as 1–4] at pH 4.5 exhibiting radii R_b from 1.6 to 2.4 μm. By using Eqs. (1), (42), (43), (44), and (45), we obtained the adhesion-induced tension γ of the membrane, the spreading pressure S, the Laplace pressure across the blister membrane ΔP, and the enriched concentration $\Delta c = c_{\rm in} - c_{\rm out}$ of solute inside the blisters, as compared to the surrounding medium. For comparison, we also included the results of measurements at the rim of the adhesion disk [line E_1 in Fig. 9(b)].

The adhesion-induced tension γ of the membrane in the blisters was found to range from 4.5×10^{-6} to 7.0×10^{-6} J/m^2, and the spreading coefficient S from 1.1×10^{-6} to 2.1×10^{-6} J/m^2. These values agree well with those at the rim of the adhesion disk, where we found $\gamma\approx4.5\times10^{-6}$ and $S\approx0.9\times10^{-6}$ J/m^2. The uniformity of γ is an important result, because it shows that the tension throughout the inhomogeneous membrane is constant, as expected for a fluid membrane. If tension gradients were present, there would be tension-induced transport of lipids, until a homogeneous tension was reached. Physically, there appears to be little difference between the contact line and the rim of the blisters. We found in this way that for pH 4.5, the ratio S/W is of the order of $\approx10^{-3}$ both for the outer rim and for the blisters. The spreading pressure in this regime is apparently completely unrelated to the specific adhesion energy W.

The physical interpretation of the ratio S/γ and the contact angle ϑ_c is in fact quite different in the regime of $|\sigma_1|$ large compared to σ_2. Suppose we assume that the adhesion disk exhausts all of the anionic lipids. Then we must demand

$$\pi R^2|\sigma_1| = 4\pi r^2\sigma_2^0, \tag{43}$$

with r the (original) radius of the vesicle and σ_2^0 the original cationic surface charge. Since $\sin\vartheta_c \cong R/r$ it follows from Young's law [Eq. (1)] that

$$S/\gamma = 1-\sqrt{1-(R/r)^2}. \tag{44}$$

Eliminating the ratio R/r by Eq. (43) gives

$$S/\gamma = 1-\sqrt{1-4\sigma_2^0/|\sigma_1|}. \tag{45}$$

The S/γ ratio is then simply set by the concentration ratio $\sigma_2^0/|\sigma_1|$ of the surface charges. To verify this claim, note that, for pH 4.5, $|\sigma_1|\approx10\sigma_2^0$ since the NBD-DODA-SA to DHDAB ratio is roughly 10:1. The value of S/γ predicted by Eq. (45) is then 0.22, while the measured S/γ value of Table II gives an S/γ value of 0.20 for pH 4.5, in good agreement. Measurement of contact angles or S/γ values in this regime simply reflects the membrane demixing and gives no information at all concerning the specific adhesion energy. We conclude that for $|\sigma_1|$ large compared to σ_2, the S/W ratio monitors the enrichment of the adhesion disk of a vesicle following adhesion-induced phase separation.

C. Long time stability of blisters

In order to check the long time stability of blisters, which were formed after adjusting the pH to the constant value 4.5, the contact area was observed for 4 h. During this time the blisters remained spherical caps. This suggests that the ions are trapped in the blisters at least over this time scale or longer. This observation enables us to obtain an upper limit of the spacing between the two adhering membranes under conditions of charge regulation. According to Fick's law, the rate of change of the total number of molecules (dN/dt), trapped in the blisters, is of the order of

$$dN/dt \cong D_{\rm sol}\Delta c(t=0)h_{\rm gap}. \tag{46}$$

where $D_{\rm sol}$ is the diffusion constant of the solute, $h_{\rm gap}$ is the intermembrane distance, and $\Delta c(t=0)$ is the initial concentration difference of ions trapped in the blisters.

This means that $\Delta c(t)\cong\Delta c(t=0)e^{-t/\tau}$ must decay exponentially in time with a time constant $\tau\cong V_B/(D_{\rm sol}h_{\rm gap})$, with V_B the blister volume. Using a typical diffusion constant $D_{\rm sol}\approx100\ \mu$m^2/s for the sucrose, citric acid, and salt ions, we find that the condition that τ must exceed 10^{-3}–10^{-4} s demands that $h_{\rm gap}$ must be of the order of Å. This is in agreement with our assumption that the two membranes adhere closely in the charge-regulated state.

D. Threshold charge density σ^*

Blistering is only expected if the minority charge density σ_2 exceeds the threshold $\sigma^* = \epsilon\kappa k_BT/4\pi e$ [see Eq. (8)]. Assuming an area of 100 Å^2 per lipid, a dielectric constant $\epsilon=80$, a Debye screening length of $\kappa^{-1}=62$ Å^2 (corresponding to an ion concentration of 5 mM), the threshold σ^* would correspond to a molar fraction of $x=7\times10^{-4}$ of charged lipids. In order to test the prediction that if σ_2 exceeds this threshold then decomposition and blistering takes place, we performed the following experiment: DMPC—cholesterol vesicles containing molar fractions of $x=7\times10^{-5}$, 7×10^{-4}, 7×10^{-3}, and 7×10^{-2} of the charged lipid DHDAB, corresponding to charge densities of $0.1\sigma^*$, $1\sigma^*$, $10\sigma^*$, and $100\sigma^*$, respectively, were prepared, and their adhesion on the supported monolayers, containing 10% of NBD-DODA-SA was examined following a pH jump from pH 2.8 to 4.5. For DHDAB molar fractions of $x=7\times10^{-4}$, 7×10^{-3} and 7×10^{-2}, blisters were formed for vesicles with contact areas larger than $25\pm5\ \mu$m^2. For vesicles with smaller contact areas, no blisters were observed. For the molar fraction of DHDAB of $x=7\times10^{-5}$, no blistering was observed. This appears to agree with the theoretical predictions, but for these vesicles contact areas larger than $25\pm5\ \mu$m^2 have not been observed and the mea-

surements do not allow one to determine the threshold correctly. Techniques with a higher lateral resolution than RICM are required.

IV. CONCLUSION

We have examined both theoretically and experimentally the adhesion of a multicomponent cationic vesicle to an anionic substrate. The study was motivated by the question of whether the physical description of adhesion of simple single-component membranes could be generalized to more realistic multicomponent membranes. The key conclusions of our work on the simple binary membranes is that if adhesion induces phase separation inside the membrane, then a quite different form of adhesion takes place which is characterized by a serious failure of the Young-Dupré law and by enrichment of the adhesion disk in those chemical constituents of the vesicle which favor vesicle-substrate bonding.

We believe that this second form of adhesion should actually be more typical for biomembrane adhesion than the first, and that the breakdown of the Young-Dupré law should be essential. The reason is as follows. A single vesicle or liposome in suspension has a tension γ which is essentially zero. Adhesion of vesicles produces a finite tension γ, in particular if the vesicle volume is fixed by solute content. From the Young-Dupré law, we would have expected that the adhesion-induced tension γ must be of the order of the specific adhesion energy W. Now, the lysis tension γ_L of vesicles is of the order of 0.1 erg/cm^2 [24]. We thus should expect that adhering vesicles will burst if W exceeds 0.1 erg/cm^2 provided the Young-Dupré law holds. van der Waals forces produce adhesion energies which are less than the lysis tension, and there is no problem. However, a patch of ''molecular bridges'' with a reasonable binding energy of $10k_BT$ or more, and a reasonable surface density exceeding 10^{-3} 1/Å^2, would have a specific adhesion energy W which would exceed 1.0 erg/cm^2. The validity of the Young-Dupré law thus would appear to be inconsistent with adhesion of intact vesicles by molecular bridging under reasonable conditions. However, we have seen for our model system that, experimentally, the Young-Dupré law is actually seriously violated, and that we can account for this failure by thermodynamic analysis. The breakdown of the Young-Dupré law produces a ''tension release'' which does allow formation of adhesive patches with $W \gg \gamma_L$, with no lysis. Although we did not find other references concerning failure of the Young-Dupré law in the literature on membrane adhesion, it is in fact well known in the literature on surfaces adhering by polymers [25].

We are aware that our conclusions are based on a comparison between an experimentally measured spreading pressure S and a theoretically computed specific adhesion energy W, based on a rather simple continuum description. It is important to recall that the adhesion energy W was computed only within a simple DH theory. We have considered corrections to the predictions of DH theory using Poisson-Boltzmann theory. Although there are indeed noticeable corrections, they certainly were not able to account for the very large difference between S and W for the tight adhesion case. Ideally, W would have been measured experimentally itself. We are however encouraged by the fact that for the single-phase regime $|\sigma_1| < \sigma_2$, the calculated W value and the measured S value were in good agreement, while the failure of the Young-Dupré law, with $S/W \approx 10^{-3}$, in the two phase region, was very serious indeed. Furthermore, the predicted blister formation and coarsening phenomena are in qualitative agreement with experiment as is the threshold surface charge σ^*.

Quantitative verification of the theory would involve a study of the phase-transition boundary $|\sigma_1| = \sigma_2$ to monitor the decrease of S/W starting at the phase boundary as predicted by Eqs. (13a) and (13b), combined with a quantitative determination of the specific adhesion energy W, for instance

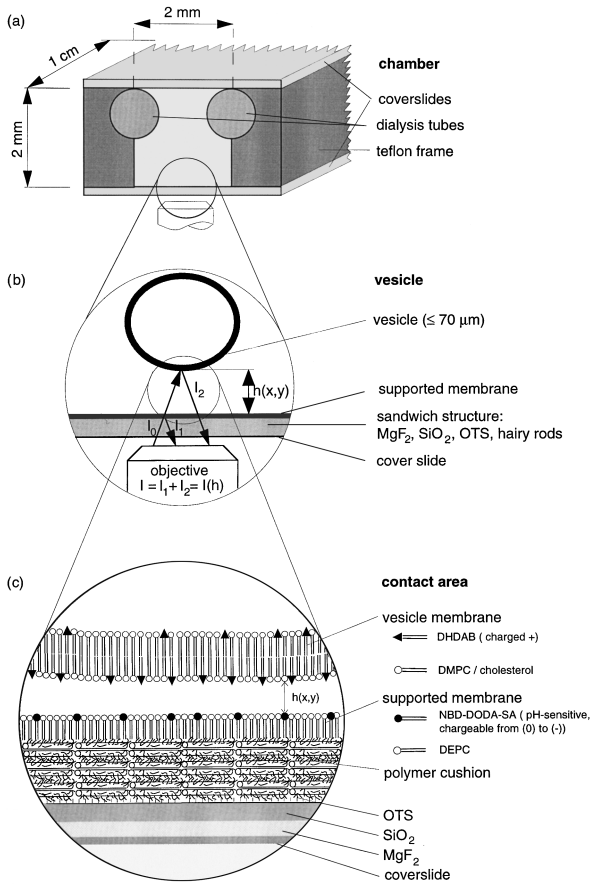

FIG. 12. Schematic drawing of measuring chamber (a), designed to change the pH of the aqueous solution inside the chamber via dialysis tubes. The chamber is formed by a teflon frame, the functionalized coverslide, serving as the bottom of the chamber, and a normal coverslide as the top. The dialysis tubes (diameter 1 mm, pore width smaller than 0.65 μm) are located close to the top coverslide, and the shortest distance between the parallel oriented tubes is 1 mm. Vesicles which are close to the bottom coverslide are observed by RICM (b). The bottom coverslide is coated with a layer of 95-nm MgF_2, which is covered by a 25-nm-thick layer of SiO_2 (c). The glass surface is rendered hydrophobic by silanization with OTS. Six layers of hairy rods form a 10-nm-thick cushion, on top of which a monolayer of DEPC and NBD-DODA-SA is deposited. The charge of the carboxy head groups of the latter can be changed from negatively charged to uncharged, and vice versa, by varying the pH of the bulk. This leads to pH-dependent electrostatic interactions of this layer with the adjacent lipid bilayer of the vesicle, which is charged positively, due to the positively charged lipid DHDAB.

by use of the Israelachvili force box. Quantitative studies also will require precise calibration of σ_1. This is currently difficult due to the fact that the bulk pH level in general differs from the pH value close to the surface of the membrane. The theoretical work could be improved by using the full Poisson-Boltzmann theory rather than the linearized Debye-Hückel theory.

We only addressed adhesion-induced phase separation in our study. Other forms of adhesion-induced phase separation are possible as well. For instance, the van der Waals interaction between substrate and vesicle is likely to favor the gel state of the membrane. Another example would be the formation of Ca^{2+} bridges between equally charged acidic membranes, which is well known to induce the fluid to gel transition of charged lipids [3]. These adhesion-induced freezings are likely to produce phase separation in a multicomponent membrane. We plan to address this question in a future study.

APPENDIX: MATERIALS AND METHODS

Materials

DEPC (*L*-α-dielaidoyl phosphatidycholine), cholesterol and DMPC (*L*-α-dimyristoyl phosphatidycholine) (all $\geqslant$99%) were purchased from Avanti Polar Lipids (Alabama). DHDAB (dihexadecyldimethyl ammonium bromide) ($\geqslant$97%) was purchased from Fluka AG (Buchse, Switzerland). The lipid NBD-DODA-SA (octadecyl-[NBD-decyl]-dimethyl ammonium succinic acid) ($\geqslant$99%) was synthesized by Ingmar Dorn in our laboratory [14]. Lipids were used without further purification. Chloroform, methanol and 1-butanol (all HPLC quality) were purchased from Fluka AG (Buchse, Switzerland). OTS (octadecyltrichlorosilane), sucrose [$\leqslant$99.5%, HPLC (high pressure liquid chromatography) quality] citric acid, sodiumchloride (NaCl) were from Sigma (Deisenhofen, Germany). Hairy rods (poly[(γ-octadecyl-*L*-glutamate)-co-(γ-methyl-*L*-glutamate)]) were synthesized by the Wegner group at the Max Planck Institute für Polymerforschung (Mainz, Germany). All lipids were dissolved in a mixture of chloroform and methanol (2:1 volume ratio), hairy rods were dissolved in chloroform (0.5 mg/ml). In order to adjust the pH, buffers were titrated by 1M NaOH (pro analysis, Riedel de Haen, Seelze, Germany) and 1-M HCl (p.a., Merck, Darmstadt, Germany). For all aqueous solutions water of millipore quality (Millipore GmbH, Eschborn, Germany) with a specific resistance of $\geqslant$18 MΩ/cm was used. Magnesiumdifluoride (MgF_2), siliconoxide (SiO), and indium tin oxide (ITO)-coated glasses were purchased from Balzers (Lichtenstein). The thickness of ITO was 120 nm, and the thickness of the coated glass was 1.1 mm. Borosilicate coverslides, D26, were products of Deutsche Spezialglas AG (Germany).

The dialysis tubes Accurel (PP, type Q3/2) were purchased from Akzo Faser AG (Wuppertal, Germany). Before mounting, dialysis tubes were hydrophylized by pumping 1-butanol into the tubes for 20 min. By closing one of their ends, the 1-butanol was squeezed through the tube pores. In a second step, water, instead of 1-butanol, was pumped through the pores of the tubes for 20 min, and finally water was pumped through the reopened tubes for 5 min.

Preparation of vesicles

The vesicles were composed of an equimolar mixture of DMPC and cholesterol, to which 1 mol % of the positively charged lipid DHDAB (the σ_2 component) was added. Vesicles were prepared by the method of electroswelling (the electrical tension was 0.1 V/cm^2, the frequency 10 Hz and the swelling time 2 h) in water containing 5-mM NaCl and sucrose, following Ref. [26]. The concentration of sucrose was adjusted to 40 mM. After swelling, the solution of vesicles was diluted by an isoosmolar citric acid buffer, containing 5-mM NaCl. The volume ratio of the vesicle solution to that of buffer suspension was 1:3.

Preparation of substrate and supported membrane

The glass support was first coated with a 95-nm-thick MgF_2 film, and subsequently with a 25-nm-thick SiO_2 film. The MgF_2 coating served the increase of the contrast of the interferometric technique (RICM) following Refs. [27] and [28]. The SiO_2 coating was deposited in order to enable the silanization of these substrates with OTS, which is necessary to generate a hydrophobic surface for the deposition of the hairy rod multilayer. The latter consisted of 6 ML, which were transferred from the film balance at a lateral pressure of 20 mN/m, following Ref. [28]. This soft polymer cushion had a thickness of 10 ± 1 nm [28].

Finally, the monolayer of negatively chargeable NBD-DODA-SA (the σ_1 component) and neutral DEPC (molar ratio 1:9) was transfered onto this cushion of hairy rods by dipping the substrate in horizontal orientation through the lipid monolayer, which was spread at the air water interface of a film balance. During the transfer, the lateral pressure was kept at 20 mN/m.

Measuring chamber

For the experiments the dialysis chamber shown in Fig. 12 was used. The bottom and the top plate consisted of two coverslides, which were separated by a teflon frame forming a volume of $10 \times 2 \times 2$ mm^3. The hairy rod multilayer and the lipid monolayer were deposited onto the bottom plate before assembling the chamber. The two dialysis tubes were oriented parallel to the long axis of the chamber at a distance of 1 mm. The bottom plate was assembled below water. The addition of the diluted vesicle solution to the water filled chamber, the positioning of the dialysis tubes, and the closing by the top plate occurred outside. The chamber was sealed by silicon grease. Before usage, the glass parts, the teflon frame, and the mounting chamber were cleaned by subsequent sonification, first in 2% Hellmanex solution and then in Millipore water, for 15 min each time.

Charging of σ_1

The experiments were started with uncharged supported membranes. At the beginning, the pH of the aqueous phases was adjusted to a value (typically pH 2.8) well below the pK_s value of the NBD-DODA-SA, which is $pK_s = 4 \pm 0.5$ in aqueous bulk solution. In order to charge the supported membrane by deprotonization of the carboxyl head groups of

the NBD-DODA-SA lipid, the pH of the outer medium was increased by continuously pumping a solution of the same composition, but higher pH, through the dialysis tubes. Typically the pH was increased by succeeding pH jumps of 0.3 pH units. This increase of the pH is accompanied by an increase of the ionic strength of the buffer, and thus a deflation of the originally spherical vesicle (of volume V_0). The change in relative volume $v = V/V_0$ with pH is $d(V/V_0)/d(\mathrm{pH}) = 0.13$. The contact area of a selected vesicle was observed with RICM, and images were recorded continuously at a rate of 25 images per second. In a separate measurement the time evolution of the pH change inside the chamber after pumping a solution with increased pH through the dialysis tubes was measured with the help of carboxyfluorescein dissolved in the aqeous medium [29].

ACKNOWLEDGMENTS

R.B. would like to thank the colleagues and students of the Physics Department for their hospitality and the Sonderforschungsbereich 266/C1 for their financial support, as well as thank the NSF under Grant No. DMR-9706646 for support. We would like to thank E. Evans, E. Frey, B. Gelbart, and F. Pincus for helpful discussions. We are also grateful to G. Wiegand for his advice concerning the preparation of the hairy rod cushion, and to I. T. Dorn, L. Schmitt, and R. Tampé for providing the lipid NBD-DODA-SA. Finally, we thank K. Eberle for his outstanding design and construction of the measuring cell. The work was supported by the Deutsche Forschungsgemeinschaft (Grant No. SFB 266, C1) and by the Fonds der Chemischen Industrie.

[1] B. Alberts *et al.*, *Molecular Biology of the Cell* (Garland, New York, 1983).
[2] See, for instance, R. Lipowsky and E. Sackkmann, *Handbook of Biological Physics* (Elsevier, Amsterdam, 1995), Vol. 1A, Chap. 1.3.
[3] E. Sackmann, FEBS Lett. **346**, 3 (1994).
[4] O. G. Mouritsen and M. Bloom, Biophys. J. **46**, 141 (1984).
[5] M. Glaser *et al.*, J. Biol. Chem. **271**, 26 187 (1996).
[6] A. Loidl-Stahlhofen *et al.*, Nature Biotechnol. **14**, 999 (1996).
[7] See, for instance, J. Israelachvili, *Intermolecular & Surface Forces* (Academic, San Diego, 1992), Chap. 12.
[8] See, for instance, R. Lipowsky and E. Sackmann, *Handbook of Biological Physics* (Ref. [2]), Vol. 1B, Chap. 11.
[9] J. Nardi *et al.*, Europhys. Lett. **37**, 371 (1997).
[10] P. G. de Gennes, Rev. Mod. Phys. **57**, 827 (1985).
[11] B. W. Ninham and A. Parsegian, J. Theor. Biol. **31**, 405 (1971).
[12] D. Y. Chan, D. J. Mitchell, and B. W. Ninham, J. Chem. Phys. **72**, 5159 (1980).
[13] V. A. Parsegian and D. Gingell, Biophys. J. **12**, 1192 (1972).
[14] See, for instance, P. Attard, D. J. Mitchell, and B. W. Ninham, J. Chem. Phys. **89**, 4358 (1988).
[15] J. F. Lennon and F. Brochard, J. Phys. (Paris) **36**, 1035 (1975).
[16] C. Isenberg, *The Science of Soap Films and Soap Bubbles* (Dover, New York, 1992).
[17] I. T. Dorn *et al.*, J. Am. Chem. Soc. **120**, 2753 (1998).
[18] W. T. Coackley *et al.*, Eur. Biophys. J. **13**, 123 (1985).
[19] A. Albersdörfer *et al.*, Biophys. J. **73**, 245 (1997).
[20] U. Seifert and R. Lipowsky, Phys. Rev. A **42**, 4768 (1990).
[21] R. Bruinsma, in Proceedings of the NATO Advanced Institute of Physics and Biomaterials, Vol. 332 of *NATO Advanced Study Institute Series B: Physics* (Kluwer, Dordrecht, 1995), p. 611.
[22] H. P. Duwe and E. Sackmann, Physica A **163**, 410 (1990).
[23] See, for instance, R. Lipowsky and E. Sackmann, *Handbook of Biological Physics* (Ref. [2]), Vol. 1A, Chap. 5.5.
[24] D. Needham *et al.*, Biochemistry **27**, 4668 (1988).
[25] E. Kramers (private communication).
[26] M. I. Angelova and D. S. Dimitrov, Faraday Discuss. Chem. Soc. **81**, 303 (1986).
[27] J. Rädler *et al.*, Phys. Rev. E **51**, 4526 (1995).
[28] G. Wiegand *et al.*, Langmuir **13**, 3563 (1997).
[29] J. Nardi, thesis, Technical University Munich, 1995 (unpublished).